Separation and Purification Technology 320 (2023) 124186

Contents lists available at ScienceDirect

Separation and Purification Technology

journal homepage: www.elsevier.com/locate/seppur

High-performance electrocatalytic reduction of CO_2 to CO by ultrathin PdCu alloy nanosheets

Jigang Wang [a,*], Guangyang Zhang [b], Huan Liu [c], Zhongfang Li [a], Likai Wang [a,e,*], John Tressel [d], Shaowei Chen [d,*]

[a] School of Chemistry and Chemical Engineering, Shandong University of Technology, Zibo, Shandong 255049, China
[b] National Engineering Research Center for Marine Aquaculture, Zhejiang Ocean University, Zhoushan, Zhejiang 316022, China
[c] Department of Chemistry, Tsinghua University 100084 Beijing China
[d] Department of Chemistry and Biochemistry, University of California, Santa Cruz, CA 95064, USA
[e] Qingdao Institute of Bioenergy and Bioprocess Technology, Chinese Academy of Sciences, Qingdao, Shandong 266101, China

ARTICLE INFO

Keywords:
CO_2 reduction
Bimetallic
Nanosheet
Binding energy
D-band center

ABSTRACT

Electrochemical reduction of carbon dioxide (CO_2RR) into fuels and chemicals is a significant step to balance the carbon cycle. For CO_2 reduction to CO, the binding energy of intermediates *COOH and *CO is crucial for the electrocatalytic activity and selectivity. Herein, we prepare a series of ultrathin and tunable PdCu alloy nanosheets by a one-pot wet chemistry process and demonstrate that the bimetallic nanosheets can improve the electronic configurations and break the inherent scaling relationship of intermediate binding energy, which leads to a high performance of CO_2RR. Specifically, Pd_1Cu_1 exhibits the best CO_2RR performance among the series, with a faraday efficiency (FE) of 97% CO at − 0.80 V vs reversible hydrogen electrode (RHE) in 0.1 M $KHCO_3$ and 96% at − 0.88 V in 1 M KOH with a current density of 521 mA cm^{-2}. This is ascribed to moderate *COOH binding and weak binding of *CO on Pd_1Cu_1, as manifested in both experimental and theoretical studies. Results from this work highlight the unique potentials of bimetallic alloy nanosheets as high-performance catalysts for electrochemical reduction of CO_2.

1. Introduction

The combustion of fossil fuels leads to the increase of carbon dioxide (CO_2) in the atmosphere, breaking the carbon cycle and causing environmental problems, such as greenhouse effect, acid rain, etc. [1,2]. Electrochemical CO_2 reduction reaction (CO_2RR) to value-added chemicals and fuels is an effective strategy to alleviate the greenhouse issues and promote a circular economy [3–7]. Among the products of CO_2RR, CO is considered as the most promising one, since it is a critical feedstock for the production of renewable fuels and chemicals, including acids, esters, and alcohols, which can replace conventional fossil-based fuels and chemicals [8–10]. However, owing to the chemical inertness of CO_2, the wide range of reduction products and competitive hydrogen evolution reaction (HER) [11,12], effective catalysts are needed to reduce the high energy barrier and improve CO selectivity for CO_2RR, which depend on the binding energy and chemisorption configuration of reaction intermediates [13]. An inherent challenge is that the intermediate bindings follow the conventional scaling relationships due to the similar surface − adsorbate bonds [14,15]. For example, the C-binding energy of the intermediates, such as *COOH and *CO, shows the same trend when the center of the d band is shifted [13], resulting in a reduced activity. For pure Pd electrodes, the strong binding energy of Pd-C bond is beneficial to reduce the Gibbs free energy of the *COOH intermediate, while the strong binding energy of *CO is not conducive to the formation of CO, resulting in a low Faraday efficiency of CO (FE_{CO}) [16–18]. This scaling relationship can be broken by the rational design and engineering of ideal catalysts that feature a moderate *COOH binding energy and weak *CO binding energy [19–21].

In recent years, bimetallic Pd-based alloy nanostructures have attracted great attention due to their tunable electronic/surface configurations, which can impact the binding energy of key reaction intermediates by manipulation of the atomic ratio in the alloy [22–25]. For instance, Pd—Au alloy catalysts have been found to exhibit a weakened Pd—C bond and balanced bindings of *COOH and *CO, leading to a high efficiency and mass activity toward CO_2RR to CO [26]. $Pd_{0.75}Ag_{0.25}$ catalysts have also been observed to display a significant

* Corresponding authors.
E-mail addresses: jgwang2008@sdut.edu.cn (J. Wang), lkwangchem@sdut.edu.cn (L. Wang), shaowei@ucsc.edu.cn (S. Chen).

https://doi.org/10.1016/j.seppur.2023.124186
Received 25 March 2023; Received in revised form 23 April 2023; Accepted 23 May 2023
Available online 26 May 2023

decrease in the binding of *CO and *H, while retain a strong binding of *COOH, which facilitates the electron-transfer kinetics toward CO production (FE_{CO} = 95.3%) [27]. With a low d-orbital vacancy, Cu has also been used to engineer Pd-based alloys and modulate the electronic effect toward well-coordinated *COOH and *CO. For instance, Cu-Pd alloys with a 1:1 atomic ratio show a high FE_{CO} of 87% at −0.90 V due to the increase of the energy barrier of the *CO protonation step, as compared to the monometallic Pd [28].

In addition, the catalytic performance can also be enhanced by structural engineering of the metallic catalysts at the nanoscale. Towards this end, two-dimensional (2D) nanostructures have been drawing extensive attention due to the relatively high surface area-to-volume ratio and high density of exposed atoms on their surface [29]. Herein, PdCu alloy nanosheets are prepared by a one-pot wet chemistry process at various Pd:Cu atomic ratios. Alloying Cu to Pd is beneficial for breaking the scaling relation between the binding energy of specific intermediates, and thus facilitates the formation of CO. Electrochemically, the PdCu alloy nanosheets exhibits an FE_{CO} over 95% with a current density of 521 mA cm^{-2} in 1 M KOH at −0.88 V. Density functional theory (DFT) calculations show that Pd_1Cu_1 exhibits the best selective production of CO among the series, due to a reduced energy barrier of CO formation.

2. Experimental

2.1. Materials

Palladium(II) acetylacetonate ($Pd(acac)_2$), copper(II) acetylacetonate ($Cu(acac)_2$), molybdenum carbonyl ($Mo(CO)_6$), trioctylphosphine oxide (TOPO), oleic acid (OA), isopropyl alcohol, N, N-dimethylformamide (DMF) and Nafion (5%) were purchased from Sigma-Aldrich. Ethanol (99.9%) was purchased from Damao. CO_2 (purity 99.995%), Ar (purity 99.99%), N_2 (purity 99.99%) and H_2 (purity 99.999%) were obtained from Zibo Baiyan Gases. DI water was obtained from a Barnstead Nanopure water purification system (18.3 MΩ cm). All materials were used without further purification.

2.2. Synthesis of PdCu alloy nanosheets

PdCu alloy nanosheets was synthesized via a modified one-pot wet chemistry process. Firstly, 5 mg (16.4 mmol) of $Pd(acac)_2$, 4.3 mg (16.4 mmol) of $Cu(acac)_2$, 6 mg (22.7 mmol) of $Mo(CO)_6$ and 63 mg (162.9 mmol) of TOPO were added into 4 mL of OA in a 50 mL round-bottom flask under sonication for 10 min, before the addition of 0.75 mL of DMF under vigorous stirring in an Ar atmosphere for 30 min. The flask

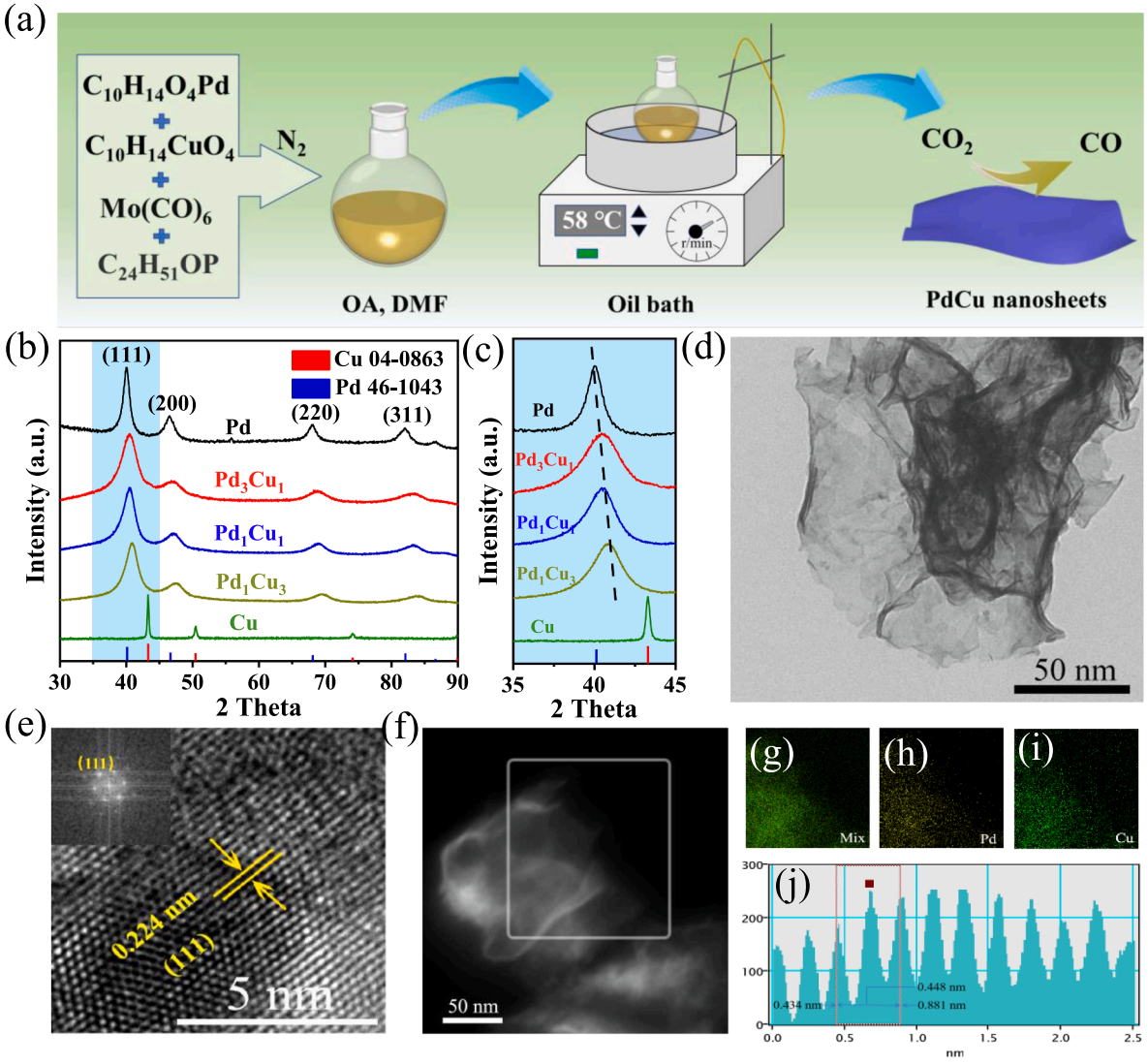

Fig. 1. (a) Schematic illustration of the preparation of PdCu alloy nanosheets, (b and c) XRD patterns of Pd_1Cu_1, (d and e) TEM and HRTEM images, (f-i) EDS elemental maps of Pd_1Cu_1 and (j) interplanar spacing.

was then heated into an oil bath at 58 ℃ for 18 h. The resulting solution was centrifuged at 8,000 rpm for 5 min, and the precipitate was collected and rinsed 3 times with DI water and ethanol. Finally, the product was desiccated in a vacuum oven (40 ℃), which denoted as Pd_1Cu_1. PdCu alloy nanosheets at other Pd/Cu atomic ratios were prepared by using the same synthetic method but with a different amount of $Cu(acac)_2$ and denoted as Pd_xCu_y. Monometallic Pd and Cu were also prepared by following the same procedure by using only $Pd(acac)_2$ or $Cu(acac)_2$ precursors.

3. Results and discussion

3.1. Characterization of the samples

The PdCu alloy nanosheets at different Pd:Cu atomic ratios were prepared by a one-pot wet chemistry process, where palladium(II) acetylacetonate ($Pd(acac)_2$) and copper(II) acetylacetonate ($Cu(acac)_2$) were reduced thermally in oleic acid and N,N-dimethylformamide, as illustrated in Fig. 1a (details in the Supporting Information). Five samples were prepared, Pd, Pd_3Cu_1, Pd_1Cu_1, Pd_1Cu_3 and Cu, and the crystalline structure was first examined by X-ray diffraction (XRD) measurements. As shown in Fig. 1b-c, one can see that the monometallic Pd sample exhibited four major diffraction peaks at $2\theta = 40.1°$, 46.6°, 68.1°, and 82.1° that can be assigned to the (111), (200), (220) and (311) crystalline planes of *fcc* Pd (PDF No. 46–1043). For the PdCu bimetallic samples, these diffraction peaks can be seen to shift to a higher angle with an increasing Cu content, suggesting the formation of Pd-Cu alloys, due to a reduced lattice spacing with Pd being replaced with smaller Cu atoms[30,31]. For instance, the four diffraction peaks of Pd_1Cu_3 appeared at 40.8°, 47.4°, 69.6°, and 83.9°, and the diffraction profile was markedly different from that of the monometallic Cu sample, which featured three diffraction peaks at $2\theta = 43.3°$, 50.4°, and 74.1°, consistent with *fcc* Cu (PDF No. 04–0836).

The surface morphology of the samples was characterized by transmission electron microscopy (TEM) measurements. As shown in Fig. 1d and Fig. S1, the samples all exhibited an ultrathin nanosheet structure. In high-resolution TEM (HRTEM) measurements (Fig. 1e), Pd_1Cu_1 can be seen to display well-defined lattice fringes with an interplanar spacing of 0.224 nm (Fig. 1j), which is in line with the (111) facets of PdCu alloy. The selected area electron diffraction (SAED) patterns of Pd_1Cu_1 were shown in the inset to Fig. 1e, which can be ascribed to the (111) crystal planes of PdCu alloys, in good agreement with results from the XRD measurements (Fig. 1b-c). This is further confirmed in elemental mapping analysis based on energy dispersive spectroscopy (EDS) where the Pd and Cu elements were evenly distributed over the entire nanosheets (Fig. 1f-i).

The elemental composition and valence states of the sample series were then examined by X-ray photoelectron spectroscopy (XPS) measurements. From the survey spectra in Fig. 2, all samples can be seen to exhibit the Pd 3d peak and Cu 2p peaks. In addition, from the integrated peak areas, the atomic contents of Pd and Cu were estimated to be 3.2 for Pd_3Cu_1, 1.2 for Pd_1Cu_1, and 0.4 for Pd_1Cu_3, consistent with the initial feed ratios (Table S1). The corresponding high-resolution Pd 3d scans are shown in Fig. 2a, which can be deconvolved into two doublets. For the monometallic Pd sample, the two doublets can be identified at 335.7/341.0 eV and 336.9/342.2 eV, due to the $3d_{3/2}$ and $3d_{5/2}$ electrons of metallic Pd^0 and Pd^{2+} species, respectively [32]. Yet, for the PdCu alloy samples, the binding energy of these two doublets can be seen to exhibit a marked red-shift with increasing Cu loading, from 335.3/340.5 eV and 336.4/341.5 eV for Pd_3Cu_1 to 335.0/340.2 eV and 336.1/341.3 eV for Pd_1Cu_1 and 334.8/340.0 eV and 335.9/341.1 eV for Pd_1Cu_3. The high-resolution Cu 2p spectra are depicted in Fig. 2b, which can also be deconvoluted into two doublets. For the monometallic Cu samples, the two doublets appeared at 931.5/951.4 eV and 933.2/953.4 eV, due to $2p_{1/2}$ and $2p_{3/2}$ electrons of metallic Cu and Cu^{2+} species, respectively [33,34]. The oxidation state of metals was probably caused by the surface partial oxidation upon exposure to air. Notably, the binding energies of these doublets were markedly higher in the PdCu samples, and increased with increasing Pd contents, 931.9/951.7 eV and 934.2/954.0 eV for Pd_1Cu_3 to 932.4/952.2 eV and 934.6/954.4 eV for Pd_1Cu_1 and 932.9/952.7 eV and 935.1/955.0 eV for Pd_3Cu_1. Taken together, these results suggest effective electron transfer from Cu to Pd, due to the formation of PdCu alloys and a lower electron negativity of Cu than that of Pd [29].

3.2. Electrocatalytic performance for CO_2RR

The electrocatalytic activity of the PdCu alloy nanosheets towards CO_2RR was then investigated in an H-type cell in a typical three-electrode setup by linear sweep voltammetry (LSV) in Ar- or CO_2–saturated 0.1 M $KHCO_3$. From Fig. 3a it can be seen that Pd_1Cu_1 displayed a markedly higher current density in CO_2-saturated 0.1 M $KHCO_3$ than in Ar-saturated 0.1 M $KHCO_3$, indicating an apparent CO_2RR activity. The corresponding product selectivity is depicted in Fig. 3b, where CO can be identified as the major product whereas H_2 and CH_4 are the minor ones. Specifically, the FE_{CO} on Pd_1Cu_1 was over 80% within a wide potential range of −0.6 to −1 V, reaching a maximum of 97% at −0.9 V. The performance was markedly lower with other samples in the series, where the maximum FE_{CO} was only about 80%, 78% and 62% for Pd_1Cu_3, Pd_3Cu_1 and Pd, respectively (Fig. S2a,b and Fig. S3a), whereas

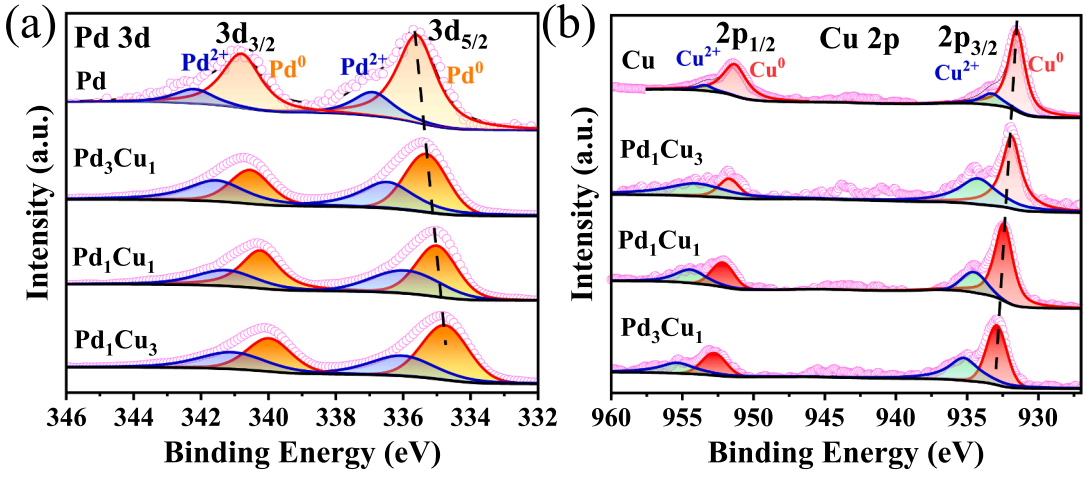

Fig. 2. High-resolution XPS profiles of the (a) Pd 3d and (b) Cu 2p electrons of PdCu alloy nanosheets. Symbols are experimental data and colored peaks are deconvolution fits.

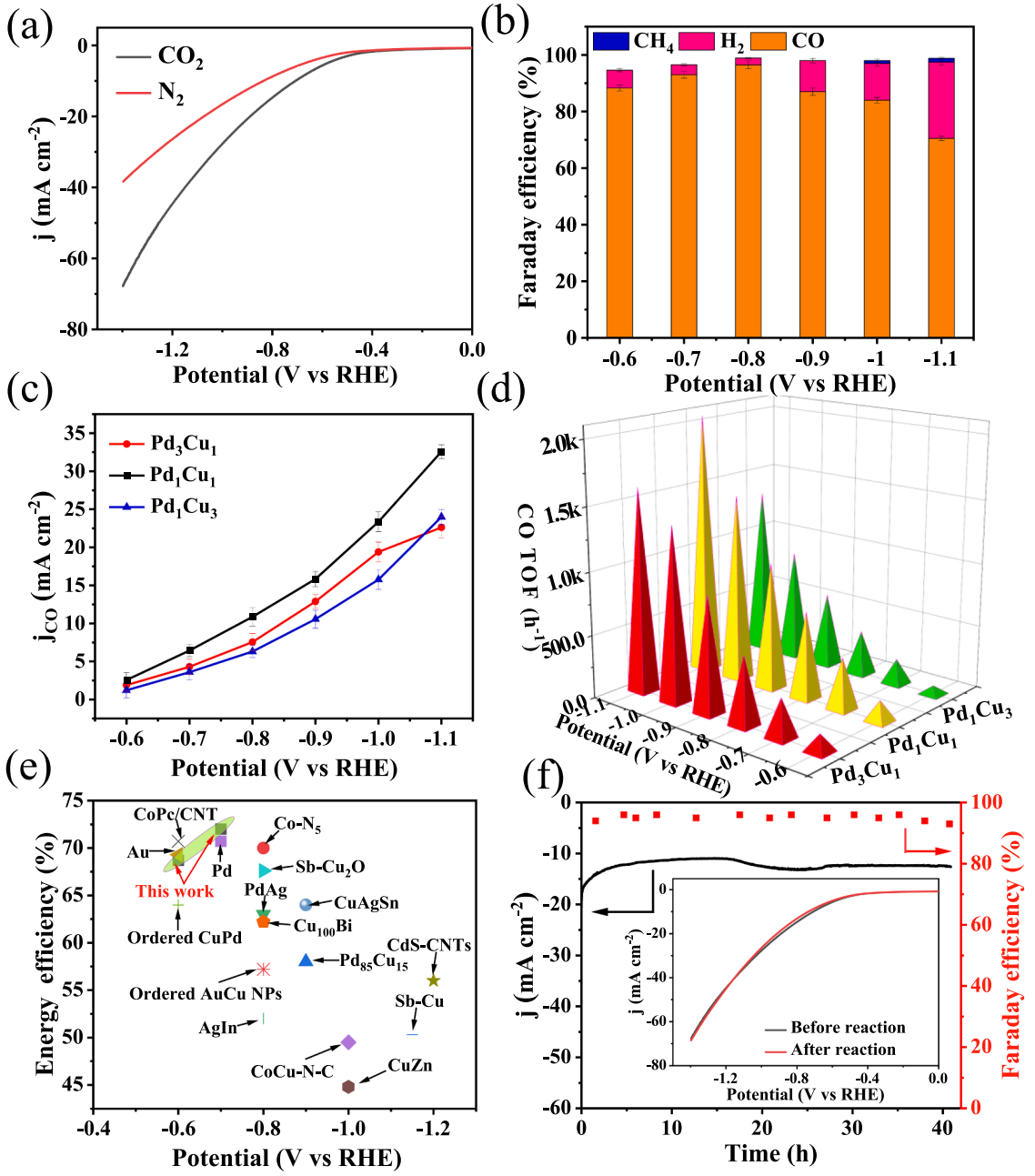

Fig. 3. (a) LSV curves of Pd_1Cu_1 in N_2– and CO_2-saturated 0.1 M $NaHCO_3$ at a scan rate of 10 mV s^{-1}, (b) FE of CH_4, CO and H_2 on Pd_1Cu_1, (c) Partial current densities and (d) TOF of CO on the PdCu alloy nanosheets, (e) Energy efficiency of CO_2 to CO of the catalysts reported in the literature, (f) Stability test of Pd_1Cu_1 at −0.8 V for 42 h. Inset shows the corresponding LSV profiles before and after the stability test.

for the monometallic Cu sample, the maximum FE_{CO} was only 27% at −0.8 V and H_2 became the major product, along with others like CH_4, C_2H_4 and HCOOH (Fig. S3d). The total current density and partial geometric current density of the products at varied applied potentials are shown in Fig. S2c-d, Fig. S3b-c and S3e-f. It can be clearly seen that Pd_1Cu_1 possessed the highest geometric current density of CO (j_{co}), reaching a maximum of 33 mA cm^{-2} at −1.1 V (Fig. 3c). This suggests that Pd_1Cu_1 stood out as the best catalyst for CO_2RR to CO among the sample series within the context of FE and current density.

The intrinsic activity of the PdCu alloy nanosheets was evaluated by normalizing the current density to the electrochemical surface area (ECSA), which was determined by double layer capacitance (Fig. S4). Pd_1Cu_1 can be seen to possess a better activity than other samples in the series, and the trend of the current density normalized to ECSA is the same as that of the geometric current density (Fig. S5). Furthermore, the Pd_1Cu_1 also shows the highest turnover frequency (TOF) value (Fig. 3d, 2064.7 h^{-1}) and the highest formation rate of CO (Fig. S6), among the catalysts. Notably, the cathodic energy efficiency (EE) of the Pd_1Cu_1 sample for CO formation was also better than results of relevant catalysts reported previously in the literature (Fig. 3e and Table S2).

The corresponding Tafel plots are shown in Fig. S7a, from which Pd_1Cu_1 can be seen to exhibit a Tafel slope (183 mV dec^{-1}) lower than those of Pd_1Cu_3 (243 mV dec^{-1}) and Pd_3Cu_1 (196 mV dec^{-1}), suggesting that the rate determining step (RDS) of CO_2RR was the generation of CO_2^{*-} and the electron-transfer kinetics was much faster on Pd_1Cu_1 than on other samples [2,35]. Indeed, in electrochemical impedance spectroscopy (EIS, Fig. S7b) measurements, Pd_1Cu_1 possesses a lower charge-transfer resistance (R_{CT}) than others. Furthermore, the current density

and Faraday efficiency of the Pd_1Cu_1 catalyst remained virtually invariant at −0.8 V for 42 h in 0.1 M $KHCO_3$ (Fig. 3f), and there was no significant change of the LSV profiles (insert Fig. 3f) and TEM image (Fig. S8), indicating excellent stability of the Pd_1Cu_1 nanosheets.

Due to the low solubility of CO_2 in aqueous solution, only a relatively low current density can be produced in an H-type cell, which limits their practical application that requires a CO partial current density of at least 100 mA cm^{-2} [36]. Thus, the catalytic activity of the Pd_1Cu_1 catalyst was also examined in a flow cell reactor in 1 M KOH electrolyte (Fig. 4a), where a small onset potential and the high current density were obtained (Fig. 4b), due to hydroxide ions can suppress the competing HER and lower the CO_2 activation energy barrier [11]. Fig. 4c shows the partial current densities and FE_{CO} at various electrode potentials, where j_{co} can be seen to increase to 521 mA cm^{-2} with an FE_{CO} of 96% at −0.88 V. The Pd_1Cu_1 catalysts also exhibited excellent stability at high current density, which remained almost unchanged at 230 mA cm^{-2}, with FE_{CO} of 97% at −0.68 V, in 1 M KOH for 17 h (Fig. 4d).

3.3. DFT theoretical calculation

Density functional theory (DFT) calculations were then performed to unravel the correlation between the catalyst structure and adsorption energetics of key reaction intermediates. The structural models are shown in Fig. S9-S10. The different electronic structures of the alloys at different compositions are related to the change of the d-band center, which impacts the adsorption strength of reaction intermediates [37]. As shown in Fig. 5a, with the increase of the Cu content, the PdCu alloys exhibit a down-shift of the d-band center from the Fermi level (E_F), suggesting a weakened binding of intermediates on the catalyst surface [38]. From Fig. 5b, it can be found that Pd exhibits strong adsorption with the intermediates of *COOH and *CO, which is not conducive to the desorption of the reaction products [35]. With the alloying of Cu to Pd, the binding energy of *COOH and *CO first decreased with the increasing content of Cu, reaching the valley at Pd_1Cu_1; yet with a further increase of the Cu content (i.e., Pd_1Cu_3 and Cu), the binding of *COOH was slightly enhanced, while the binding of *CO stayed virtually unchanged. In a conventional scaling relationship, the variation of the adsorption energy of *CO and *COOH is correlated to each other, and *COOH binding cannot be optimized without affecting the *CO adsorption [21]. Yet, the results presented above suggest that manipulation of the elemental composition of the PdCu alloys can retain the moderate binding of *COOH and concurrently weakened binding of *CO at appropriate Cu contents, thus breaking the scaling relationship. The weakened adsorption of *CO is conducive to the desorption of CO, and moderate adsorption of *COOH is beneficial to the subsequent reaction. This coordination between *CO and *COOH is of great importance to boost the kinetics toward CO production. In addition, the binding of *H is gradually weakened with the increase of the Cu content, thus suppressing the competition of HER with the appropriate Cu contents, another feature that is conducive to CO_2RR electrocatalysis (Fig. S11a).

Analysis of the molecular orbital overlap can be used to further explain the interaction between reaction intermediates and catalytic active sites. Fig. 5d-e depicts the projected density of states (PDOS) of the C in chemisorbed *COOH and *CO and metal atoms on catalysts, and Fig. S11b shows that of *H. As shown in Fig. 5d, there is a large overlap between the C 2p and Pd d orbitals, indicating a strong interaction between C and Pd [39,40]. With the introduction of Cu, the overlap decreased significantly, indicating weakened binding of *COOH; yet with an excessive Cu content, the overlap actually became slightly enhanced, indicating that the binding of *COOH was somewhat strengthened. In the case of *CO, the overlap area decreased first and then remained basically unchanged with the increase of Cu content, indicating that the binding of *CO decayed first and then stayed virtually unchanged. These different variations further illustrate the breaking of the conventional scaling relationship in PdCu alloys. In addition, as the Cu content increased, a decreasing overlap can be observed between

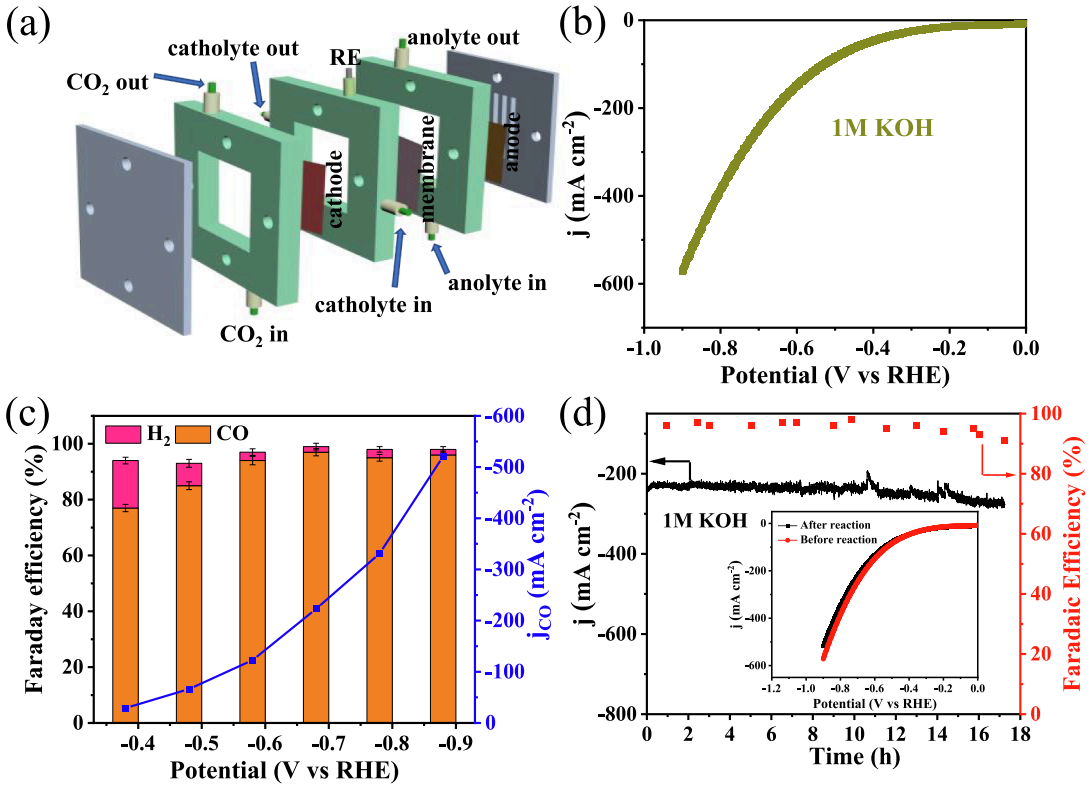

Fig. 4. (a) Schematic illustration and (b) polarization curves of Pd_1Cu_1 in 1 M KOH, (c) FE and partial current density of CO_2RR on Pd_1Cu_1 in 1 M KOH solution, (d) Long-term i-t profiles in 1 M KOH electrolyte.

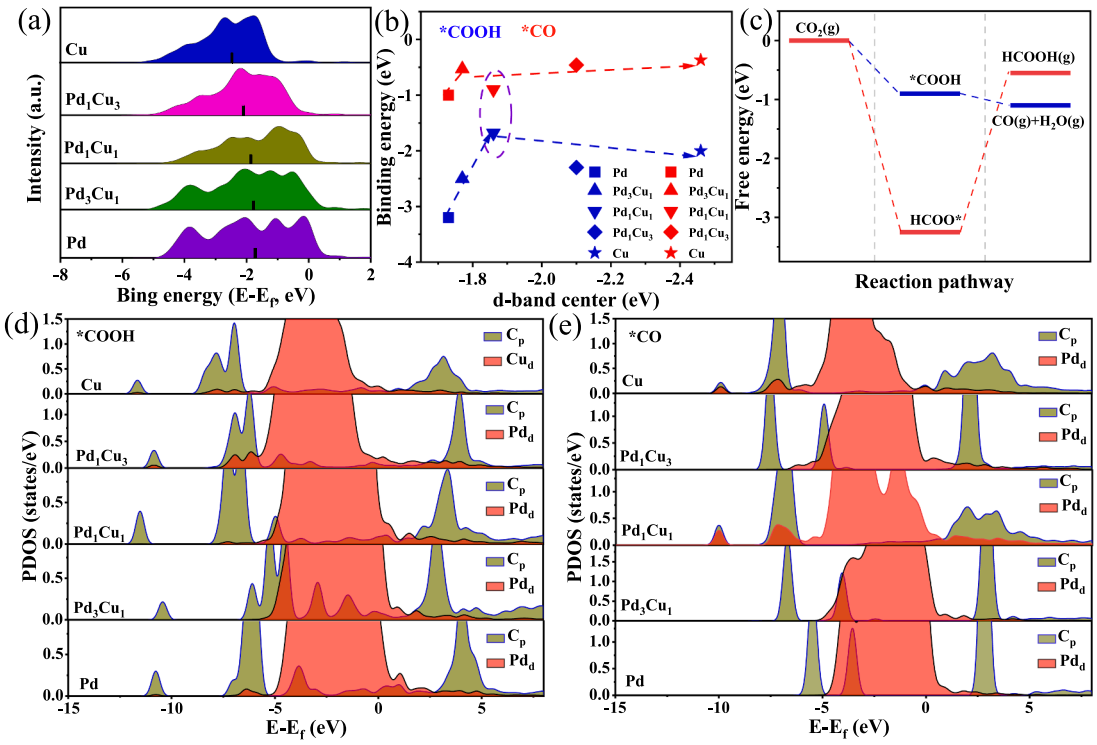

Fig. 5. (a) Projected density of states (PDOS) of different catalysts. Gray dashed line indicates E_F; black bar indicates the d band center, (b) Binding energies of *COOH and *CO on PdCu alloy nanosheets, (c) Free energy profiles of CO_2RR on Pd_1Cu_1, PDOS plots of (d) C atom in *COOH, (e) C atom in *CO with Pd atom in monometallic Pd, PdCu alloys and Cu atom in monometallic Cu surfaces.

the H s and Pd d orbitals over the PdCu surface (Fig. S11b).

To unravel the energetics and reaction pathways of CO_2RR to CO and formate, the free energy diagrams on Pd_1Cu_1 are constructed and shown in Fig. 5c. It can be seen that the entire reaction pathway of CO generation is spontaneous and exothermic on Pd_1Cu_1, indicating that CO formation is energetically preferred. For other catalysts, certain energy barriers need to be overcome in the process of CO generation (Fig. S12a). The free energy of HER on PdCu is shown in Fig. S12b. Too strong adsorption of hydrogen may lead to occupation of the active site, whereas too weak adsorption will be conducive to HER and compromise the CO_2RR activity [35]. However, the Pd_1Cu_1 shows only a moderate adsorption of hydrogen (−0.18 eV), which not only suppresses the HER process, but also provides sufficient adsorbed hydrogen needed for the reduction of CO_2. In summary, results from the DFT calculations suggest that the Pd_1Cu_1 exhibits the optimal electronic structure for the selective reduction of CO_2 to CO, among the present sample series.

4. Conclusion

In summary, a series of ultrathin and tunable PdCu alloy nanosheets were prepare by a one-pot wet-chemistry process. Results from spectroscopic and theoretical studies demonstrated that the resulting nanosheets improved the electronic configurations and broke the inherent scaling relationship of the binding energy of key reaction intermediates. Specifically, the Pd_1Cu_1 sample exhibited a high FE_{CO} of 97% at −0.8 V and a current density of 33 mA cm^{-2} at −1.1 V. In a flow cell and 1 M KOH electrolyte, a current density of 521 mA cm^{-2} and an FE_{CO} of 96% were obtained at −0.88 V. Furthermore, results from DFT calculations showed that the conventional scaling relationship of intermediates was broken at high Cu contents in the PdCu alloys, where a moderate *COOH binding and negligible *CO binding led to a high performance in the selective production of CO. Such fundamental insights may be exploited for the rational design and engineering of high-performance catalysts for electrochemical energy conversion.

Data availability

Data will be made available on request.

CRediT authorship contribution statement

Jigang Wang: Investigation, Methodology, Validation, Writing – original draft. **Guangyang Zhang:** Formal analysis, Data curation. **Huan Liu:** Data curation. **Zhongfang Li:** Data curation. **Likai Wang:** Supervision, Conceptualization, Data curation. **John Tressel:** Data curation. **Shaowei Chen:** Supervision, Data curation, Writing – review & editing.

Declaration of Competing Interest

The authors declare that they have no known competing financial interests or personal relationships that could have appeared to influence the work reported in this paper.

Data availability

Data will be made available on request.

Acknowledgements

This work is supported by National Natural Science Foundation of China (No. 21805170), Qingdao Postdoctoral Innovation Project (No. QDBSH20220202031).

Appendix A. Supplementary material

Supplementary data to this article can be found online at https://doi.org/10.1016/j.seppur.2023.124186.

References

[1] J. Hansen, P. Kharecha, M. Sato, V. Masson-Delmotte, F. Ackerman, D.J. Beerling, P.J. Hearty, O. Hoegh-Guldberg, S.L. Hsu, C. Parmesan, J. Rockstrom, E.J. Rohling, J. Sachs, P. Smith, K. Steffen, L. Van Susteren, K. von Schuckmann, J.C. Zachos, Assessing "dangerous climate change": required reduction of carbon emissions to protect young people, future generations and nature, PLoS One 8 (2013) e81648.

[2] J. Wang, S. Ning, M. Luo, D. Xiang, W. Chen, X. Kang, Z. Jiang, S. Chen, In-Sn alloy core-shell nanoparticles: in-doped SnO_x shell enables high stability and activity towards selective formate production from electrochemical reduction of CO_2, Appl. Catal. B 288 (2021), 119979.

[3] B. Jiang, X.-G. Zhang, K. Jiang, D.-Y. Wu, W.-B. Cai, Boosting formate production in electrocatalytic CO_2 reduction over wide potential window on Pd Surfaces, J. Am. Chem. Soc. 140 (8) (2018) 2880–2889.

[4] Y.-X. Duan, F.-L. Meng, K.-H. Liu, S.-S. Yi, S.-J. Li, J.-M. Yan, Q. Jiang, Amorphizing of Cu nanoparticles toward highly efficient and robust electrocatalyst for CO_2 reduction to liquid fuels with high faradaic efficiencies, Adv. Mater. 30 (2018) 1706194.

[5] L. Dai, Q. Qin, P. Wang, X. Zhao, C. Hu, P. Liu, R. Qin, M. Chen, D. Ou, C. Xu, S. Mo, B. Wu, G. Fu, P. Zhang, N. Zheng, Ultrastable atomic copper nanosheets for selective electrochemical reduction of carbon dioxide, Sci. Adv. 3 (2017) e1701069.

[6] L. Jia, M. Sun, J. Xu, X. Zhao, R. Zhou, B. Pan, L.u. Wang, N.a. Han, B. Huang, Y. Li, Phase-dependent electrocatalytic CO_2 reduction on Pd3Bi nanocrystals, Angew. Chem. Int. Ed. 60 (40) (2021) 21741–21745.

[7] T. Cao, R. Lin, S. Liu, W.-C. Cheong, Z. Li, K. Wu, Y. Zhu, X. Wang, J. Zhang, Q. Li, X. Liang, N. Fu, C. Chen, D. Wang, Q. Peng, Y. Li, Atomically dispersed Ni anchored on polymer-derived mesh-like N-doped carbon nanofibers as an efficient CO_2 electrocatalytic reduction catalyst, Nano Res. 15 (5) (2022) 3959–3963.

[8] S. Sato, K. Saita, K. Sekizawa, S. Maeda, T. Morikawa, Low-Energy Electrocatalytic CO_2 Reduction in Water over Mn-Complex Catalyst Electrode Aided by a Nanocarbon Support and K^+ Cations, ACS Catal. 8 (5) (2018) 4452–4458.

[9] E.E. Benson, C.P. Kubiak, A.J. Sathrum, J.M. Smieja, Electrocatalytic and homogeneous approaches to conversion of CO_2 to liquid fuels, Chem. Soc. Rev. 38 (1) (2009) 89–99.

[10] S. Zhu, B. Jiang, W.-B. Cai, M. Shao, Direct observation on reaction intermediates and the role of bicarbonate anions in CO_2 electrochemical reduction reaction on Cu surfaces, J. Am. Chem. Soc. 139 (44) (2017) 15664–15667.

[11] Q. Gong, P. Ding, M. Xu, X. Zhu, M. Wang, J. Deng, Q. Ma, N. Han, Y. Zhu, J. Lu, Z. Feng, Y. Li, W. Zhou, Y. Li, Structural defects on converted bismuth oxide nanotubes enable highly active electrocatalysis of carbon dioxide reduction, Nat. Commun. 10 (2019) 2807.

[12] W. Luc, C. Collins, S. Wang, H. Xin, K. He, Y. Kang, F. Jiao, Ag–Sn bimetallic catalyst with a core-shell structure for CO_2 reduction, J. Am. Chem. Soc. 139 (5) (2017) 1885–1893.

[13] A. Vasileff, C. Xu, Y. Jiao, Y. Zheng, S.-Z. Qiao, Surface and interface engineering in copper-based bimetallic materials for selective CO_2 electroreduction, Chem. 4 (8) (2018) 1809–1831.

[14] A.A. Peterson, J.K. Nørskov, Activity descriptors for CO_2 electroreduction to methane on transition-metal catalysts, J. Phys. Chem. Lett. 3 (2) (2012) 251–258.

[15] J.S. Yoo, R. Christensen, T. Vegge, J.K. Nørskov, F. Studt, Theoretical insight into the trends that guide the electrochemical reduction of carbon dioxide to formic acid, ChemSusChem. 9 (4) (2016) 358–363.

[16] D. Gao, H.u. Zhou, F. Cai, J. Wang, G. Wang, X. Bao, Pd-containing nanostructures for electrochemical CO_2 reduction reaction, ACS Catal. 8 (2) (2018) 1510–1519.

[17] W. Sheng, S. Kattel, S. Yao, B. Yan, Z. Liang, C.J. Hawxhurst, Q. Wu, J.G. Chen, Electrochemical reduction of CO_2 to synthesis gas with controlled CO/H_2 ratios, Energ. Environ. Sci. 10 (5) (2017) 1180–1185.

[18] M.u. Li, J. Wang, P. Li, K. Chang, C. Li, T. Wang, B.o. Jiang, H. Zhang, H. Liu, Y. Yamauchi, N. Umezawa, J. Ye, Mesoporous palladium–copper bimetallic electrodes for selective electrocatalytic reduction of aqueous CO_2 to CO, J. Mater. Chem. A 4 (13) (2016) 4776–4782.

[19] P. Chen, Y. Jiao, Y.-H. Zhu, S.-M. Chen, L.i. Song, M. Jaroniec, Y. Zheng, S.-Z. Qiao, Syngas production from electrocatalytic CO_2 reduction with high energetic efficiency and current density, J. Mater. Chem. A 7 (13) (2019) 7675–7682.

[20] K. Sun, T. Cheng, L. Wu, Y. Hu, J. Zhou, A. Maclennan, Z. Jiang, Y. Gao, W. A. Goddard, Z. Wang, Ultrahigh mass activity for carbon dioxide reduction enabled by gold-iron core–shell nanoparticles, J. Am. Chem. Soc. 139 (44) (2017) 15608–15611.

[21] Y. Li, Q. Sun, Recent advances in breaking scaling relations for effective electrochemical conversion of CO_2, Adv. Energy Mater. 6 (2016) 1600463.

[22] D. Bagchi, S. Sarkar, A.K. Singh, C.P. Vinod, S.C. Peter, Potential- and Time-Dependent Dynamic Nature of an Oxide-Derived PdIn Nanocatalyst during Electrochemical CO_2 Reduction, ACS Nano 16 (4) (2022) 6185–6196.

[23] M. Gholinejad, F. Khosravi, M. Afrasi, J.M. Sansano, C. Nájera, Applications of bimetallic PdCu catalysts, Catalysis, Sci. Technol. 11 (8) (2021) 2652–2702.

[24] T. Zeng, X. Meng, H. Huang, L. Zheng, H. Chen, Y. Zhang, W. Yuan, L.Y. Zhang, Controllable synthesis of web-footed PdCu nanosheets and their electrocatalytic applications, Small 18 (2022) 2107623.

[25] W. Bi, X. Li, R. You, M. Chen, R. Yuan, W. Huang, X. Wu, W. Chu, C. Wu, Y. Xie, Surface immobilization of transition metal ions on nitrogen-doped graphene realizing high-efficient and selective CO_2 reduction, Adv. Mater. 30 (2018) 1706617.

[26] X. Yuan, L. Zhang, L. Li, H. Dong, S. Chen, W. Zhu, C. Hu, W. Deng, Z.-J. Zhao, J. Gong, Ultrathin Pd–Au Shells with Controllable Alloying Degree on Pd nanocubes toward carbon dioxide reduction, J. Am. Chem. Soc. 141 (12) (2019) 4791–4794.

[27] J. Zeng, W. Zhang, Y. Yang, D. Li, X. Yu, Q. Gao, Pd–Ag Alloy electrocatalysts for CO_2 reduction: composition tuning to break the scaling relationship, ACS Appl. Mater. Interfaces 11 (2019) 33074–33081.

[28] Y. Mun, S. Lee, A. Cho, S. Kim, J.W. Han, J. Lee, Cu-Pd alloy nanoparticles as highly selective catalysts for efficient electrochemical reduction of CO_2 to CO, Appl. Catal. B 246 (2019) 82–88.

[29] N. Yang, Z. Zhang, B. Chen, Y. Huang, J. Chen, Z. Lai, Y. Chen, M. Sindoro, A.-L. Wang, H. Cheng, Z. Fan, X. Liu, B. Li, Y. Zong, L. Gu, H. Zhang, Synthesis of ultrathin PdCu alloy nanosheets used as a highly efficient electrocatalyst for formic acid oxidation, Adv. Mater. 29 (2017) 1700769.

[30] D. Tan, J. Zhang, J. Shi, S. Li, B. Zhang, X. Tan, F. Zhang, L. Liu, D. Shao, B. Han, Photocatalytic CO_2 Transformation to CH_4 by Ag/Pd Bimetals Supported on N-Doped TiO_2 nanosheet, ACS Appl. Mater. Interfaces 10 (29) (2018) 24516–24522.

[31] D. Bin, B. Yang, K.e. Zhang, C. Wang, J. Wang, J. Zhong, Y. Feng, J. Guo, Y. Du, Design of PdAg hollow nanoflowers through galvanic replacement and their application for ethanol electrooxidation, chemistry – A, Eur. J. 22 (46) (2016) 16642–16647.

[32] R. Lin, X. Ma, W.-C. Cheong, C. Zhang, W. Zhu, J. Pei, K. Zhang, B. Wang, S. Liang, Y. Liu, Z. Zhuang, R. Yu, H. Xiao, J. Li, D. Wang, Q. Peng, C. Chen, Y. Li, PdAg bimetallic electrocatalyst for highly selective reduction of CO_2 with low COOH* formation energy and facile CO desorption, Nano Res. 12 (11) (2019) 2866–2871.

[33] B. Yu, J. Diniz, K. Lofgren, Q. Liu, R. Mercado, F. Nichols, S.R.J. Oliver, S. Chen, Copper/carbon nanocomposites for electrocatalytic reduction of oxygen to hydrogen peroxide, ACS Sustain. Chem. Eng. 10 (47) (2022) 15501–15507.

[34] K.e. Liu, Y. Song, S. Chen, Oxygen reduction catalyzed by nanocomposites based on graphene quantum dots-supported copper nanoparticles, Int. J. Hydrogen Energy 41 (3) (2016) 1559–1567.

[35] J. Wang, J. Zou, X. Hu, S. Ning, X. Wang, X. Kang, S. Chen, Heterostructured intermetallic CuSn catalysts: high performance towards the electrochemical reduction of CO_2 to formate, J. Mater. Chem. A 7 (2019) 27514–27521.

[36] D.M. Weekes, D.A. Salvatore, A. Reyes, A. Huang, C.P. Berlinguette, Electrolytic CO_2 reduction in a flow cell, Acc. Chem. Res. 51 (4) (2018) 910–918.

[37] J.K. Nørskov, T. Bligaard, J. Rossmeisl, C.H. Christensen, Towards the computational design of solid catalysts, Nat. Chem. 1 (1) (2009) 37–46.

[38] D. Kim, J. Resasco, Y. Yu, A.M. Asiri, P. Yang, Synergistic geometric and electronic effects for electrochemical reduction of carbon dioxide using gold–copper bimetallic nanoparticles, Nat. Commun. 5 (2014) 4948.

[39] G. Wen, D.U. Lee, B. Ren, F.M. Hassan, G. Jiang, Z.P. Cano, J. Gostick, E. Croiset, Z. Bai, L. Yang, Z. Chen, Orbital interactions in Bi-Sn bimetallic electrocatalysts for highly selective electrochemical CO_2 reduction toward formate production, Adv. Energy Mater. 8 (2018) 1802427.

[40] F.M. Hassan, R. Batmaz, J. Li, X. Wang, X. Xiao, A. Yu, Z. Chen, Evidence of covalent synergy in silicon–sulfur–graphene yielding highly efficient and long-life lithium-ion batteries, Nat. Commun. 6 (2015) 8597.